Meccanica (2012) 47:469–482
DOI 10.1007/s11012-011-9460-y

Numerical investigation on the influence of surface texture on the performance of hydrodynamic journal bearing

S. Kango · D. Singh · R.K. Sharma

Received: 24 March 2010 / Accepted: 15 June 2011 / Published online: 5 July 2011

Abstract Many researchers have adopted various techniques for improving the performance characteristics of journal bearing. Apart from other parameters, incorporation of different forms of surface texture (sinusoidal, dimple, spherical etc.) on bearing or shaft also helps to increase the load carrying capacity and reduce the friction coefficient etc. in the journal bearing. Present study investigates the influence of different forms of surface texture on finite journal bearing which has been considered in the form of negative texture (micro cavities) at different locations of bearing surface. The Governing equations are solved numerically through finite difference approach for analysis of texture effects on bearing characteristics. It has been observed that the presence of micro cavities at different locations of bearing surface help in enhancing the bearing performance. It has also been found that the negative half wave texture enhances the bearing performance more in comparison to full wave texture on bearing surface.

Keywords Journal bearing · Textured surface · Hydrodynamic lubrication · Finite difference method · Load carrying capacity · Half wave texture · Full wave texture

S. Kango · D. Singh · R.K. Sharma (✉)
Mechanical Engineering Department,
National Institute of Technology, Hamirpur, HP, 177005,
India
e-mail: rajesh@nitham.ac.in

S. Kango
e-mail: s3kango@yahoo.com

List of symbols

c	Radial clearance (μm)
d	Depth of cavity (m or μm)
d_b	Bearing diameter (m)
d_j	Journal diameter (m)
e	Relative eccentricity of the journal
F	Friction force (N)
F_T	Texture friction force (N)
f	Friction coefficient
f_T	Texture friction coefficient
h	Nominal film thickness (m)
H	Texture film thickness $= h + \delta_f \& h + \delta_h$ (m)
I	Number of nodes in X-direction
J	Number of node in Y-direction
K	Number of iterations
l	Length of bearing (m)
N	Shaft speed (rpm)
O_b	Bearing center
O_j	Journal or the shaft center
P	Textured bearing pressure (MPa)
P_s	Bearing pressure (MPa)
r	Radius of shaft (m)
U	Shaft speed (m/sec)
u	Lubricant velocity in x-direction (m/sec)
w	Width of cavity (m)
W	Load carrying capacity (N)

W_T	Texture load carrying capacity
$h_{\min}$	Minimum film thickness $= [c * (1 - \varepsilon)]$ (m)
HI, *HII*, *HIII*	Half wave texture for Configuration I, II, III
FI, *FII*, *FIII*	Full wave texture for Configuration I, II, III

Greek Symbols

τ	Shear stress (Pa)
θ	Angular direction (degree)
$\Delta\theta$	Cavity span
ε	Eccentricity ratio
η	Lubricant viscosity (Pa·s)
$\delta_f \& \delta_h$	Surface texture variation for full and half wave respectively (m)

1 Introduction

Hydrodynamic bearings have been used in different capacities for wide range of applications since long. The expanding range of tribological applications, from the traditional industrial machinery to recent applications in micro fabrication has revived the importance and interest in the related field. Researchers have adopted suitable conditions/parameters for enhancing fluid film bearings' performance.

Performance of hydrodynamic bearings has been found to have considerable influence of the bonding surfaces these posses. The surfaces may have asperities which are associated with roughness or cavities which are related to texture. The roughness may be random or deterministic in nature. The random roughness in hydrodynamic bearings may be introduced because of dust or foreign particles, additives in the lubricant, machining processes, and wear or tear at high speeds. The study of random roughness was first introduced by Tzeng and Saibel [1], subsequently various authors [2–7] have studied the influence of roughness on the performance of hydrodynamic journal bearings and it has been reported that the roughness influences the bearing performance. The roughness is thus sometimes also introduced intentionally on the bearings surface. With the advent of latest machining and fabrication techniques, researchers have started to focus on investigating the influence of cavities on the performance characteristics of hydrodynamic bearings. Few such techniques include laser surface texturing [8], novel dressing technique [9], chemical etching [10] and special grinding processes [11] etc. With the help of these techniques, it is now possible to produce microstructures on journal bearing surfaces to improve the overall tribological performance including reduction in friction, thereby improvement in reliability; increase in the pressure and load carrying capacity.

Bearing performance gets influenced due to sinusoidal roughness as has been investigated by Burton [12], Mitsuya et al. [13], Tonder [14], Letalleur [15], Huynh [16], Burstein [17, 18] and Kumar [19]. On the other hand researchers have also investigated the effects of various parameters such as cavity depth, cavity width, number of cavities, and location of cavities while studying the influence of surface texture geometry on bearing performance. Buscaglia et al. [20] have investigated the influence of very small texture amplitude and period while assuming no cavitation on infinitely wide thrust bearings. The authors concluded that the texture which maximizes the load for a given minimum clearance has no texture at all (i.e. smooth shape) and that the texture which minimizes the friction coefficient is again a smooth case. Rahmani et al. [21] studied the effect of variations of the geometrical parameters of square-shaped dimples on the tribological characteristics namely load capacity, the friction force, and the friction coefficient of partial surface-textured parallel slider bearings. The authors concluded that for partial textured surfaces, increasing the number of dimples would not help in improving either the load capacity or the friction coefficient in a pure hydrodynamic lubrication mode. Murthy et al. [22] developed a numerical model to study the effect of texture location, texture size, and density on air bearing sliders for large Knudsen numbers. Tala-ighil et al. [23] analyzed two cases, first one in which the shaft is assumed to be smooth and rigid and the second one in which the bearing surface is numerically textured with spherical dimples. The numerical results indicate that textures affect the most important bearing characteristics viz: film thickness, pressure distributions, axial film flow, and frictional torque. The analyses of spherically dimpled surface indicate that appropriate selection of size, depth, and number of dimples may affect bearing characteristics. Sinanoglu et al. [24] used threaded textured shaft surfaces to compare the experimental result with theoretical ones. The authors concluded that the load carrying capacity is significantly increased with threaded shaft surfaces when compared to the shafts with non-textured

surfaces. Tonder [25] pointed out that introduction of roughness at inlet of a sliding surface can generate extra pressure and thus support higher load, this has also been confirmed by Cupillard et al. [26].

According to De Kraker et al. [27], the use of a Reynolds equation to study the effects of texture will be valid if dimple depth is greater than minimum film thickness of the lubricant in the fluid film lubrication. Whereas Cupillard et al. [26] reported that for low eccentricity ratio the dimple depth is to be less than minimum film thickness. In another study, Brizmer et al. [28] investigated the influence of laser surface texture on parallel thrust bearing and concluded that parallel plate thrust pad has the capability of carrying load due to textured surface. The authors also reported that the dimple (cavity) depth should be about the same as that of the film thickness for best performance of the bearing. Authors also concluded that increased load carrying capacity could be caused by local cavitation at the diverging part of surface grooves. In the diverging part of the groove, cavitation may occur leading to a two-phase flow. This two-phase flow will then enter the convergent part of the groove. To achieve a net pressure build up this flow must be transformed to a single phase liquid flow. Because of the groove and film geometry, this can only be achieved if an additional amount of liquid is supplied from outside the groove. This finding was also confirmed by Shalin et al. [29] and Fowel et al. [30]. In practical cases, it is unclear how this liquid supply to dimples is achieved, especially when side leakage is considered. That is why there is a possibility that cavitation has a limited effect. Arghir et al. [31] have done CFD (computational fluid dynamics) analysis of fluid flow between parallel surfaces with relative speeds. One of the surfaces considered by the authors contains a groove which is represented by three different geometries and they concluded that there is a net pressure build up which is caused by the combined effect of the presence of a groove and of the increasing Reynolds number. Authors have also shown that Stokes equations are inadequate to predict pressure build-up with the presence of macro-roughness as inertia effects can be of importance. Similar finding were reported by Sahlin et al. [29] who have presented a study on optimization of the geometry. The authors pointed that fluid inertia was the main contribution to load carrying capacity, which increases with increasing depth and width of the groove. Above certain aspect ratio a vortex appears in the groove and load carrying capacity saturates. Cupillard et al. [32] explained a mechanism of pressure build up in a convergent gap due to texture. Authors have found that the mechanism of pressure build up in a convergent gap between two sliding surfaces due to texture is similar to that obtained with variation of convergence ratio for smooth surfaces. Brajdic-Mitidieri et al. [33] reported that cavitation at the pocket inlet occurs only at very low bearing convergence ratios (convergence ratio in the case of thrust bearing and it becomes eccentricity ratio in the case of journal bearing). Etsion [34] has presented a comprehensive review work on LST and its applications. The author emphases that the micro dimples can serve either as micro-hydrodynamic bearing in case of full or mixed lubrication, a micro reservoir for lubricant in cases of starved lubrication conditions, or a micro-trap for wear debris in either lubricated or dry sliding.

Different surface roughness models (Random roughness model, Sinusoidal model, cylindrical model, Dimple type model etc.) have been adopted by different researchers to conclude that the surface roughness or texture improves the bearing performance. In the present work therefore, Negative full and half wave rectifier equations are used for establishing surface texture and also to study the influence of such texture. The pattern of texture considered in this work has not come to the notice of the authors from any reported research work.

2 Numerical model

2.1 Governing equation

For a steady-state and laminar flow, incompressible oil and isothermal condition; Reynolds equation in cylindrical coordinates for texture bearing surface is:

$$\frac{\partial}{\partial\theta}\left(H^3\frac{\partial P}{\partial\theta}\right)+r^2\frac{\partial}{\partial y}\left(H^3\frac{\partial P}{\partial y}\right)=6\eta r\left(U\frac{dH}{d\theta}\right) \quad (1)$$

where θ and y are the coordinates in radial and longitudinal directions, P is hydrodynamic pressure for texture bearing and H is film thickness for texture bearing whereas, η, r and U are notations for lubricant's viscosity, shaft radius and shaft speed respectively.

2.2 Bearing performance parameters

The following performance parameters are calculated for texture journal bearing: the load carrying capacity

(W_T), the friction force (F_T) on the journal, and the friction coefficient (f_T) on the journal. The listed performance parameters are obtained as:

$$W_T = \int_0^l \int_0^{2\pi} Pr d\theta dy \tag{2}$$

$$\text{Percentage variation in load} = [(W_T - W)/W] * 100 \tag{3}$$

$$F_T = \int_0^l \int_0^{2\pi} \tau r d\theta dy \tag{4}$$

where shear stress, $\tau = (\frac{H}{2r})(\frac{\partial P}{\partial \theta}) + (\frac{\eta U}{H})$

$$\text{Percentage variation in friction force} = [(F_T - F)/F] * 100 \tag{5}$$

Load carrying capacity and friction force are obtained numerically through double integration by Simpson's $1/3^{\text{rd}}$ rule.

The coefficient of friction for textured bearing is computed as:

$$f_T = F_T / W_T \tag{6}$$

$$\text{Percentage variation in friction coefficient} = [(f_T - f)/f] * 100 \tag{7}$$

In above relations W, F, and f are load carrying capacity, friction force, and friction coefficient for smooth bearing respectively.

2.3 Boundary conditions

The boundary condition for the Reynolds equation for the smooth and texture bearings is [23]:

$$P = 0 \text{ at } \theta = 0^\circ, 360^\circ$$
$$P = 0 \text{ and } \frac{\partial p}{\partial \theta} = 0 \text{ at the rupture limits of the film lubricant.} \tag{8}$$

3 Texture model

The texture in the present case has been taken to be of negative nature at different locations i.e. by extruding the bearing surface at Configuration I, II and III. In order to obtain the negative texture the conventional sinusoidal wave is converted to negative wave by using Fourier series adopted from Gupta and Kumar [35].

Two types of negative texture obtained from (9) and (10) have been considered in the present work. In cylindrical coordinates, (9) gives negative full wave texture which is obtained by converting positive half of sinusoidal wave to negative half as shown in Fig. 1(a) and (10) gives negative half wave texture which is obtained by converting positive half of sinusoidal wave to negative half and negative half of sinusoidal wave to zero as shown in Fig. 1(b).

The negative full and half wave rectifier equation is given below as:

$$\delta_f = \left(\frac{4 * d}{\pi}\right)\left(\sum_{n=2,4,6,\ldots,\infty} \frac{\cos(\frac{n*\pi*r*\theta}{w})}{n^2 - 1}\right) - \left(\frac{2 * d}{\pi}\right), \tag{9}$$

$$\delta_h = \left(\frac{2 * d}{\pi}\right)\left(\sum_{n=2,4,6,\ldots,\infty} \frac{\cos(\frac{n*\pi*r*\theta}{w})}{n^2 - 1}\right) - \left(\frac{d}{\pi}\right) - \left(\frac{d * \sin(\frac{\pi*r*\theta}{w})}{2}\right) \tag{10}$$

where, $\delta_f \& \delta_h$ = Surface texture variation for full and half wave respectively, m; w = cavity width = (Length of cavity section)/Number of cavities; d = cavity depth, m; n = Even Integers i.e. 2, 4, 6, 8, 10, 12, ... In this work, maximum number of terms (n) = 100000; r = Radius of shaft, m.

Resultant equation for film thickness H of textured surface is obtained by using (9) and (10) as:

$$H = h + abs(\delta_f), \tag{11a}$$

$$H = h + abs(\delta_h) \tag{11b}$$

where

$$h = c\ (1 + \varepsilon \cos\theta) \tag{12}$$

where 'c' is the radial clearance, 'ε' = e/c is the eccentricity ratio and 'e' is the relative eccentricity of the journal.

4 Computational method

For the numerical solution of Reynolds equation (1), the Finite Difference Method/Scheme (FDM) has been

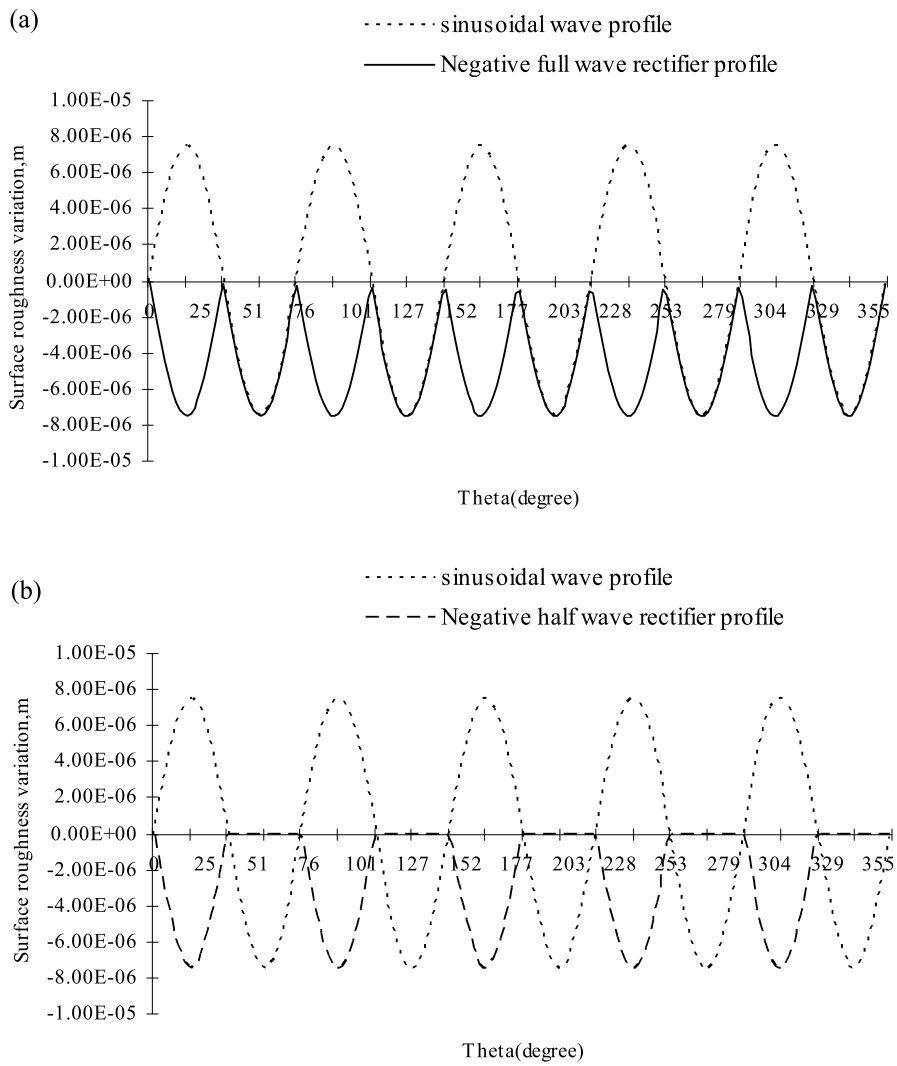

Fig. 1 Schematic diagram for (**a**) sinusoidal wave and full wave profile; (**b**) sinusoidal wave and half wave profile

used. In finite difference scheme, the differential equation has been solved numerically. The first order derivative and second order derivative in (1) has been discretized by second order central difference scheme.

After application of the FDM, the resulting discretized form of Reynolds equation (1) takes the form:

$$P_{i,j} = [(A_2(P_{i-1,j} + P_{i+1,j}) + A_3(P_{i,j-1} + P_{i,j+1}) + A_4(P_{i+1,j} - P_{i-1,j})(H_{i+1} - H_{i-1}) - A_5(H_{i+1} - H_{i-1})] \quad (13)$$

where,

$$A_1 = \frac{r^2\Delta\theta^2 + \Delta y^2}{r^2\Delta\theta^2\Delta y^2}; \quad A_2 = \frac{H_i^3}{2A_1 r\Delta\theta^2};$$

$$A_3 = \frac{H_i^3}{2A_1\Delta y^2}; \quad A_4 = \frac{3H_i^2}{8A_1 r\Delta\theta^2};$$

$$A_5 = \frac{3U\eta}{2A_1}; \quad \Delta\theta = \frac{2\pi}{I-1}; \quad \Delta y = \frac{l}{J-1}$$

where $P_{i,j}$ is the pressure at any mesh point (i, j); $P_{i+1,j}\,P_{i-1,j}\,P_{i,j+1}\,P_{i,j-1}$ are the pressures at the four adjacent points; $\Delta\theta$ and Δy are the mesh size, whereas I and J represent the number of nodes in angular and

Y direction respectively. In this work, 200 nodes have been considered in θ as well as in Y direction. The results computed have been found to be grid independent.

It is seen that the pressure at any mesh point (i, j) is expressed in terms of pressure of four adjacent points. To start with iteration method the pressures at all the mesh points are assumed and those at the boundaries are set. Equation (13) is then solved for all the mesh points.

The error at point (i, j) is

$$(\text{Error})_{i,j} = \text{R.H.S. of (13)} - P_{i,j}$$

The new pressures can be computed using a successive over relaxation method as:

$$P_{i,j} = (Pi, j)_{\text{old}} + (\text{Error})_{i,j} * \text{over relaxation factor}$$

In the present work, the pressure is computed iteratively through Gauss-Seidal method with an over relaxation factor of 1.7 as it has been reported to lie between 1.5 and 1.85 [23].

The process will be repeated till the specific accuracy is attained by a convergence criterion as:

$$\sum\sum \left| \frac{(P_{i,j})_K - (P_{i,j})_{K-1}}{(P_{i,j})_K} \right| < 0.0001 \qquad (14)$$

where K represent the number iteration.

For Iso-viscous analysis, the numerical procedure is also shown in the flow chart (Fig. 3).

4.1 Validation of the smooth model

Validation of present results has been done with those of Tala-ighil et al. [23] while considering similar conditions given as:

(1) angular speed of the journal = 625.4 rad/s;
(2) journal radius = 0.0315 m;
(3) bearing length = 0.063 m;
(4) radial clearance = 0.00003 m;
(5) lubricant viscosity = 0.0035 Pa·s;
(6) Number of nodes taken: $I = 391$ and $J = 142$.
(7) Mesh size used: $\Delta\theta = 0.016103$ and $\Delta y = 0.0004468$

The results presented in Table 1 have been found to be matching considerably well for the study of two eccentricity ratios ($\varepsilon = 0.601$ and $\varepsilon = 0.901$).

5 Results and discussions

Many investigators (Tala-ighil [23], Tonder [25], Cupillard [26] etc.) used the concept of surface texture in the form of microcavities and concluded that these are responsible for influencing the lubricant film thickness; such a variation is depicted in Fig. 4. It has been observed that lubricant film thickness (H) increases with negative texture. It is a known fact that the lubricant film thickness for smooth bearing is dependent upon radial clearance (c), eccentricity ratio (ε) and the angular position (θ). On substituting $\varepsilon = 0$ in (12), we have $h = c$, it means that the film thickness is equal to radial clearance; no converging gap is created hence no hydrodynamic pressure will generate. Thus, the friction coefficient for smooth bearing goes to infinity. On the contrary, the friction coefficient of the texture bearing has finite value for $\varepsilon = 0$ since the cavities are able to sustain a load because in texture bearing as the film thickness depends on surface texture variation δ.

In the present work, the input parameters have been taken from Kumar [19] and presented in Table 2. The journal bearing surface is divided for both texture into three configurations w.r.t. cavity span ($\Delta\theta$) i.e. Configuration I, II and III (Fig. 2b and Fig. 2c). As discussed earlier, the cavity width is the ratio of length

Table 1 Smooth journal bearing characteristics

Journal bearing characteristics	Results of Tala-ighil et al. [23]		Present results	
	$\varepsilon = 0.601$	$\varepsilon = 0.901$	$\varepsilon = 0.601$	$\varepsilon = 0.901$
Load/amplitude of the external force, W (N)	12600	81591	12663	82084
Maximum pressure, P_s (MPa)	7.70	83.58	7.70	83.60
Minimum film thickness, $h_{\min}$	11.96	2.97	11.97	2.97
Friction torque (N m)	1.217	–	1.210	–
Rupture angle (deg)	203.5	–	204.0	–

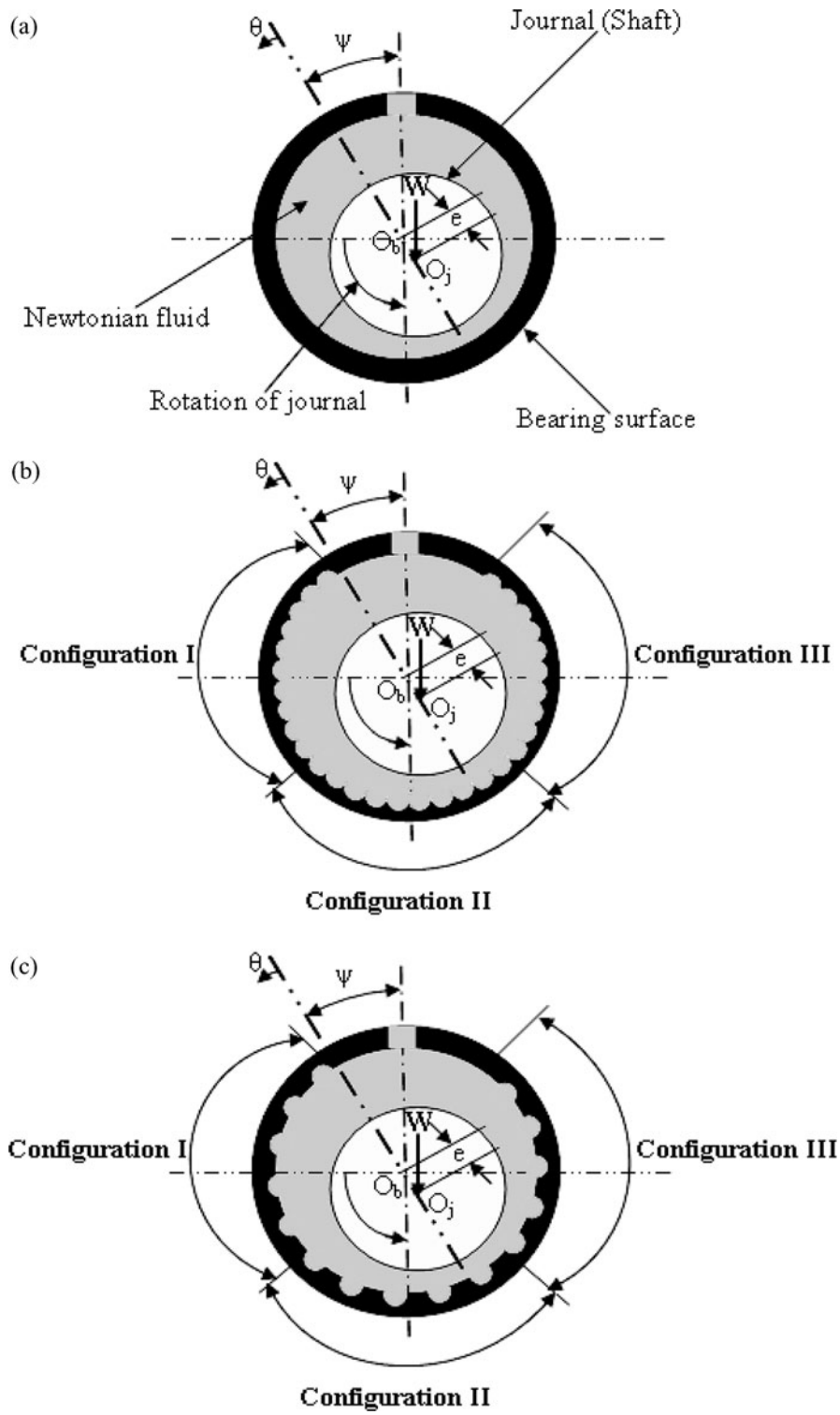

Fig. 2 Schematic diagram for (**a**) smooth journal bearing; (**b**) negative full wave texture at different locations; (**c**) negative half wave texture at different locations

Table 2 Input parameters

Sr. No.	Description	Symbol/notation	Value	Unit (SI)
1	Bearing length	l	0.1	m
2	Shaft radius	r	0.05	m
3	Radial clearance	c	0.0001	m
4	Dynamic viscosity	η	0.04	Pa·s.

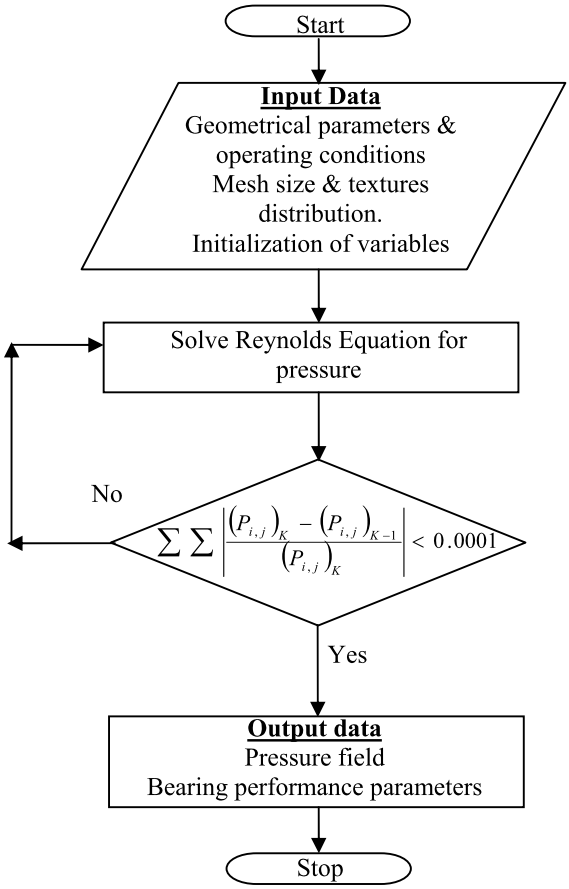

Fig. 3 Flow chart

of cavity section to number of cavities. It suggests that the cavity width can be changed in two ways. In the first case by changing the length of cavity or texture section while keeping the number of cavities constant and in the second one by changing the number of cavities with constant cavity or texture span. In the present work, both the methods are used for calculating the cavity width and their effects on bearing performance are presented one by one.

5.1 First approach: by changing the cavity or texture span while keeping number of cavities constant

Five texture spans i.e. $\Delta\theta_1 = 71°$, $\Delta\theta_2 = 84°$, $\Delta\theta_3 = 94°$, $\Delta\theta_4 = 105°$, and $\Delta\theta_5 = 116°$ have been considered in the present case. By changing these texture spans, the corresponding width of cavities and the location of cavities gets changed which is presented in Table 3. It is observed that in Configuration I for $w = 0.007$ m, the first cavity on the bearing surface

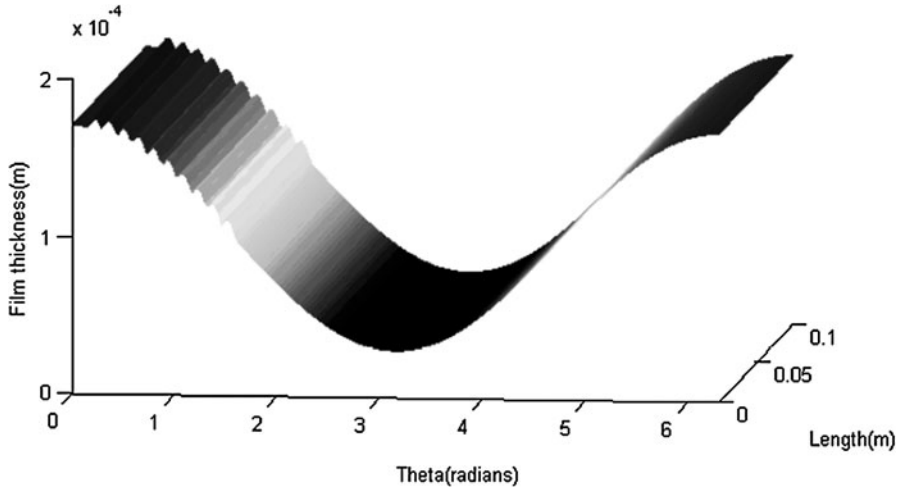

Fig. 4 3-D film thickness for full wave equation at Configuration I ($\varepsilon = 0.7$, $c = 100$ μm, $d_j = 0.1$ m, $l/d_j = 1.0$, $d = 0.0000075$ m, $w = 0.007$ m)

occurs at 10° and last cavity i.e. the tenth one occurs at 94° (= 10° + 84°). The number of cavities is set equal to 10 in each configuration.

According to De Kraker et al. [27], the use of a Reynolds equation to study the effects of texture is valid if ratio $\frac{d}{h_{\min}} > 1$ exists, whereas according to Cupillard et al. [26] the ratio $\frac{d}{h_{\min}} > 1$ is valid only for high eccentricity ratio when the textures are located in the maximum pressure region, whereas, when the textures are located just down stream of the maximum film at low eccentricity ratios, the ratio $\frac{d}{h_{\min}} \leq 1$ will be valid. Comparison of bearing performance parameters corresponding to different configurations for different surface texture has been depicted in Table 4 and Table 5 at high and low eccentricity ratios ($\varepsilon = 0.7$ and 0.3); and for $\frac{d}{h_{\min}} = 1.1$ and 0.5 respectively from above discussion.

It can be observed from Table 4 that the load and friction force decreases, whereas friction coefficient increases with increasing width of cavity or cavity span ($\Delta\theta$) in Configuration I, while this phenomenon is reversed for Configuration III for both type of surface texture. It is also found that the bearing performance characteristics for Configuration I and III has not been improving for any cavity span at this eccentricity ratio. This may happen due to incremental thickness influenced by textures in Configuration I and III, which ultimately causes to reduce the bearing pressures at this eccentricity ratio. The positive results for journal bearing has been observed for Configuration II at cavity span ($\Delta\theta_2 = 84°$) or cavity width ($w = 0.007$ m) at high eccentricity ratio for $\frac{d}{h_{\min}} > 1$. Cupillard et al. [26] also concluded that at high eccentricity ratio and dimple depth greater than minimum film thickness, the bearing performance improves when cavities are located at maximum pressure region. Therefore, in this work at Configuration II, the cavities have been considered to vary from 94° to 178° and this corresponds to the maximum pressure region.

Table 5 shows that for Configuration I (or inlet surface of bearing) the bearing performance improves in comparison to other types of configurations at low eccentricity ratio for $\frac{d}{h_{\min}} \leq 1$. At low eccentricities the phenomenon of micro cavitation prevails due to the presence of texture which is instrumental in enhancing the bearing performance in Configuration I. This finding is also confirmed by Tonder [25], Cupillard et al. [26], Murthy et al. [22], and Fowel et al. [30]. The results presented in Tables 4 and 5 have been computed for high and low eccentricity ratios for both types of textures considered in the present study. It can be seen that the bearing performance reduces in Configuration I and III, while in Configurations II, it gets enhanced for both types of texture at high eccentricity ratio. Whereas, the bearing performance improves in Configuration I for both types of textures at low eccentricity ratio. Owing to above discussion, further analysis has been carried out with cavity span $\Delta\theta_2 = 84°$ ($w = 0.007$ m) for Configuration II and with cavity span $\Delta\theta_5 = 116°$ ($w = 0.01$ m) for Configuration I.

Table 3 Details of cavity configurations, initiation of cavity, θ, and angle spanned, $\Delta\theta$, (given in brackets)

$\frac{d}{h_{\min}} = 1.1$	Configuration I	Configuration II	Configuration III
$w = 0.006$ m	10° (71°)	81° (71°)	152° (71°)
$w = 0.007$ m	10° (84°)	94° (84°)	178° (84°)
$w = 0.008$ m	10° (94°)	104° (94°)	198° (94°)
$w = 0.009$ m	10° (105°)	115° (105°)	220° (105°)
$w = 0.010$ m	10° (116°)	126° (116°)	242° (116°)

Table 4 Comparison for bearing performance parameters for ten cavities and different cavity span ($\frac{d}{h_{\min}} = 1.1$, $\varepsilon = 0.7$)

Configuration I	w (m)	% variation in W		% variation in F		% variation in f	
		Half wave	Full wave	Half wave	Full wave	Half wave	Full wave
$\Delta\theta_1 = 71°$	0.006	−0.97	−1.30	−0.17	−0.45	+0.80	+0.86
$\Delta\theta_2 = 84°$	0.007	−2.37	−3.18	−0.43	−0.86	+2.00	+2.39
$\Delta\theta_3 = 94°$	0.008	−3.96	−5.49	−0.66	−1.28	+3.43	+4.46
$\Delta\theta_4 = 105°$	0.009	−5.64	−8.27	−0.89	−1.72	+5.03	+7.14
$\Delta\theta_5 = 116°$	0.010	−6.96	−11.17	−1.08	−2.19	+6.32	+10.11
Configuration II							
$\Delta\theta_1 = 71°$	0.006	−10.77	−14.87	−1.60	−3.06	+10.30	+13.87
$\Delta\theta_2 = 84°$	0.007	+11.80	+8.10	−1.72	−4.76	−12.10	−11.90
$\Delta\theta_3 = 94°$	0.008	−23.72	−28.40	−5.03	−14.82	+24.50	+18.97
$\Delta\theta_4 = 105°$	0.009	−24.89	−53.50	−6.15	−18.97	+24.94	+74.22
$\Delta\theta_5 = 116°$	0.010	−21.60	−52.80	−6.76	−20.50	+18.93	+68.60
Configuration III							
$\Delta\theta_1 = 71°$	0.006	−22.11	−61.70	−4.85	−17.13	+22.15	+116.35
$\Delta\theta_2 = 84°$	0.007	−8.62	−22.32	−3.54	−11.05	+5.28	+14.57
$\Delta\theta_3 = 94°$	0.008	−0.05	0.29	−2.32	−6.44	−2.27	−6.16
$\Delta\theta_4 = 105°$	0.009	−0.37	−0.22	−1.35	−3.67	−0.99	−3.46
$\Delta\theta_5 = 116°$	0.010	−0.31	−0.20	−0.80	−2.23	−0.48	−2.03

5.1.1 *Influence of cavity depth (d) on Configuration II and I*

Tables 6 and 7 present the influence of cavity depth for Configuration II and I on high and low eccentricity ratios. It has been observed that with an increase in cavity depth, the percentage load and friction force increases whereas percentage friction coefficient gets reduced for Configuration II. On the other hand for Configuration I, friction force also reduces. It can therefore be concluded that high cavity depth would improve the bearing performance for both the configurations and both types of surface textures. With the increase in cavity depth, the tendency of lubricant to flow from one cavity to another decreases, which let to more suction of lubricant inside the bearing. This causes to increase the % variation in load in both the cases.

It has been also found that the percentage load increases more for half surface texture at Configuration II, whereas there is more increment in percentage load at Configuration I for full wave surface texture.

5.1.2 *Influence of eccentricity ratio (ε) in Configuration I, II and III*

Figure 5 presents a comparison of the results for pressure variation at different eccentricity ratios of 0.1, 0.2 and 0.3 for both types of rough bearings in Configuration I and for smooth bearing. Value of '*d*' has been set to 0.0000075 m and wavelength has been kept as

Table 5 Comparison for bearing performance parameters for ten cavities and different cavity span ($\frac{d}{h_{\min}} = 0.5, \varepsilon = 0.3$)

Configuration I	w (m)	% variation in W		% variation in F		% variation in f	
		Half wave	Full wave	Half wave	Full wave	Half wave	Full wave
$\Delta\theta_1 = 71°$	0.006	+2.94	+8.33	−0.38	−1.06	−3.22	−8.67
$\Delta\theta_2 = 84°$	0.007	+1.38	+7.06	−0.61	−1.56	−1.96	−8.52
$\Delta\theta_3 = 94°$	0.008	+1.10	+7.59	−0.76	−1.98	−1.84	−8.89
$\Delta\theta_4 = 105°$	0.009	+1.77	+8.57	−0.91	−2.39	−2.64	−10.09
$\Delta\theta_5 = 116°$	0.010	+2.38	+9.06	−1.10	−2.90	−3.40	−10.96
Configuration II							
$\Delta\theta_1 = 71°$	0.006	−7.61	−4.55	−1.29	−3.07	+6.84	+1.55
$\Delta\theta_2 = 84°$	0.007	−11.79	−14.78	−1.85	−4.66	+11.27	+11.87
$\Delta\theta_3 = 94°$	0.008	−24.29	−41.08	−2.50	−6.06	+29.92	+55.19
$\Delta\theta_4 = 105°$	0.009	−27.29	−59.71	−2.82	−7.77	+33.65	+128.91
$\Delta\theta_5 = 116°$	0.010	−25.79	−57.24	−3.20	−8.62	+30.45	+113.69
Configuration III							
$\Delta\theta_1 = 71°$	0.006	−21.92	−41.97	−1.98	−5.87	+25.53	+62.22
$\Delta\theta_2 = 84°$	0.007	−8.71	−14.89	−1.92	−5.47	+45.00	+11.07
$\Delta\theta_3 = 94°$	0.008	−4.13	−3.95	−1.84	−5.01	+2.39	−1.11
$\Delta\theta_4 = 105°$	0.009	−4.81	−4.20	−1.63	−4.40	+3.34	−0.14
$\Delta\theta_5 = 116°$	0.010	−3.85	−2.03	−1.39	−3.78	+2.56	−1.79

Table 6 Influence of cavity depth on bearing performance parameters in Configuration II ($\Delta\theta = 84°$, $w = 0.007$ m)

Eccentricity ratio	$\frac{d}{h_{\min}}$	% variation in W		% variation in F		% variation in f	
		Half wave	Full wave	Half wave	Full wave	Half wave	Full wave
$\varepsilon = 0.7$	1.1	+11.80	+8.10	−1.72	−4.76	−12.10	−11.89
	1.2	+17.49	+10.35	−1.43	−4.47	−16.10	−13.43
	1.3	+24.85	+12.77	−1.06	−4.09	−20.75	−14.95
	1.4	+34.38	+15.33	−0.61	−3.64	−26.03	−16.44
	1.5	+46.78	+18.04	−0.07	−3.11	−31.92	−17.91

Table 7 Influence of cavity depth on bearing performance parameters in Configuration I ($\Delta\theta = 116°$, $w = 0.010$ m)

Eccentricity ratio	$\frac{d}{h_{\min}}$	% variation in W		% variation in F		% variation in f	
		Half wave	Full wave	Half wave	Full wave	Half wave	Full wave
$\varepsilon = 0.3$	0.20	+1.24	+4.41	−0.59	−1.43	−1.80	−5.59
	0.50	+2.38	+9.06	−1.10	−2.90	−3.40	−10.96
	0.70	+4.64	+12.11	−1.19	−3.50	−5.58	−13.93
	1.0	+11.67	+16.90	−1.09	−4.03	−11.43	−17.91

0.006 m. A positive effect on pressure distribution can be observed on different eccentricity ratios from the results obtained. The asperities are highly responsible for generation of high-pressure gradient in this case. From Fig. 5, it is also observed that with the increment in eccentricity ratio, the texture pressure profile

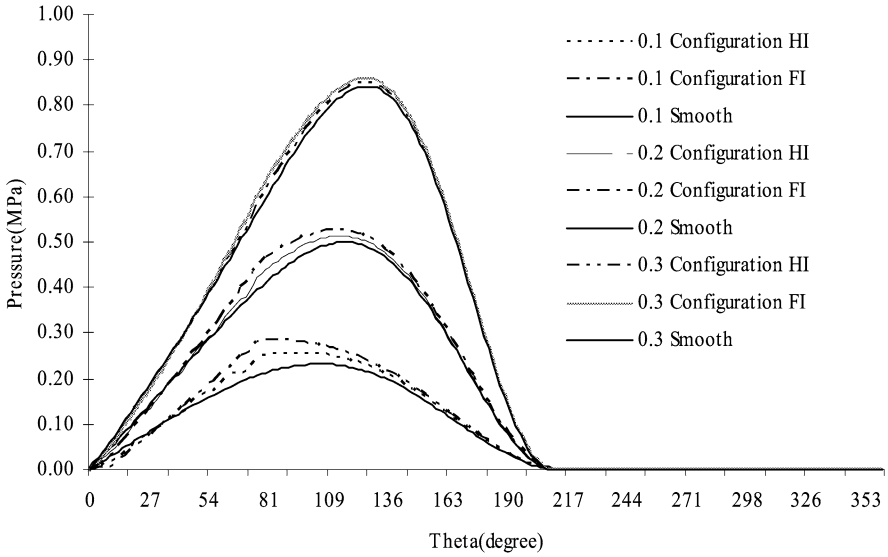

Fig. 5 Pressure variations in the Configuration I at different eccentricity ratios for both rough bearings ($c = 100$ μm, $\eta = 0.04$ Pa·s, $d_j = 0.1$ m, $l/d_j = 1.0$, $w = 0.006$ m, $N = 1000$ rpm, $d = 0.0000075$ m, eccentricity ratios 0.1, 0.2, 0.3)

Table 8 Influence of number of cavities on bearing performance parameters

	Number of cavities	Wavelength of cavity (m)	% variation in W		% variation in F		% variation in f	
			Half wave	Full wave	Half wave	Full wave	Half wave	Full wave
Configuration I	10	0.010	+11.67	+16.90	−1.09	−4.03	−11.43	−17.91
($\Delta\theta = 116°$,	12	0.0080	−5.09	+7.28	−1.48	−4.57	+3.07	−11.05
$\varepsilon = 0.3$, $d/h_{\min} = 1.0$)	14	0.0070	−16.70	+2.89	−1.78	−4.82	+17.90	−7.49
	18	0.0056	−18.18	+1.98	−1.74	−5.10	+20.12	−5.65
Configuration II	10	0.0070	+46.78	+18.04	−0.07	−3.11	−31.92	−17.91
($\Delta\theta = 84°$,	12	0.0060	−22.63	−5.72	−3.32	−6.33	+24.95	−0.65
$\varepsilon = 0.7$, $d/h_{\min} = 1.5$)	14	0.0050	−38.06	−15.35	−3.87	−7.65	+55.22	+9.10
	18	0.0040	−48.07	−17.30	−4.64	−8.10	+83.61	+9.89

comes closer the smooth pressure profile at high value of eccentricity ratio and there is decrement in texture pressure profile corresponding to Configuration I for both cases. It is also found that the pressure profile for half wave texture bearing lies between full wave and smooth bearings. As discussed earlier, if we put $\varepsilon = 0$ in (12), then no hydrodynamic pressure is generated. It means that there is less generation of hydrodynamic pressure at low eccentricity ratios for smooth case which is also depicted in Fig. 5. We also know that with the increase of eccentricity ratio, the lubricant film thickness decreases which causes to increase the bearing pressures. But due to texture there is the formation of convergent and divergent zone inside the cavity, which causes to generate the hydrodynamic pressure (or more suction of oil) at zero or low eccentricity ratios. But with the increase of eccentricity ratio the suction of oil reduce which causes to decrease the bearing pressures as shown in Fig. 5 and also explained by Murthy et al. [22] and Etsion [34].

5.2 Second approach: by changing the number of cavities while keeping the cavity span constant

Results have been presented in this section for variation in the number of cavities (i.e. 10, 12, 14, and 18) in a fixed cavity span (116° for Configuration I, 84° for Configuration II). It has been observed that the bearing

performance for full and half texture bearing in Configuration I and II is the best with 10 numbers of cavities as depicted in Table 8.

6 Conclusions

Different types of negative texture (microcavities) have been considered on journal bearing surface at different locations and the influences of cavity width and that of cavity depth on bearing performance have been investigated. The presence of negative texture helps in increasing the lubricant film thickness, which causes to decrease the friction force.

Following are the broad outcomes of present study:

1. Enhanced bearing performance has been observed in Configuration I with cavity span of 116° ($w = 0.01$ m) and dimple depth less than minimum film thickness, whereas for Configuration II it has been observed with cavity span of 84° ($w = 0.007$ m) and dimple depth greater than minimum film thickness for both type of surface texture.
2. Load carrying capacity increases by about 11.67% for half and 16.9% for full texture bearing at $\varepsilon = 0.3$ corresponding to Configuration I for $\frac{d}{h_{\min}} = 1.0$, cavity width of 0.006 m, and number of cavities as 10 whereas, the friction coefficient reduces by about 11.43% for half and 17.91% for full textured bearing.
3. For Configuration II, load carrying capacity increases by about 46.78% for half and 18.04% for full texture bearing corresponding to eccentricity ratio 0.7, for $\frac{d}{h_{\min}} = 1.5$, and cavity width 0.007 m when the number of cavities are taken as 10.

From above points it can be concluded that both type of surface texture may be fruitful in decreasing the friction force and the friction coefficient in the journal bearing. Since very low eccentricity ratios ($\varepsilon = 0.1$ to 0.3) are not normally considered in practical applications, therefore, Configuration II and half wave texture are best for improving the bearing performance as compared to other Configurations and full wave texture. Though the results presented here are for iso-viscous conditions, these present an idea for implementation of this concept in the thermal conditions also.

References

1. Tzeng ST, Saibel E (1967) Surface roughness effect on slider bearing lubrication. ASLE Trans 10:334–338
2. Christensen H (1969-70) Stochastic models for hydrodynamic lubrication of rough surfaces. Proc Inst Mech Eng 184(1):1013–1025
3. Patir N, Cheng HS (1978) An average flow model for determining effects of three-dimensional roughness on partial hydrodynamic lubrication. ASME J Lubr Technol 100:12–17
4. Patir N, Cheng HS (1979) Application of average flow model to lubrication between rough sliding surfaces. ASME J Lubr Technol 101:220–230
5. Yuanzhong H, Lingqing Z (1989) A study of the film formation for a rough slider bearing. Wear 132(1):23–38
6. Jeng YR (1990) Experimental study of the effects of surface roughness on friction. Tribol Trans 33(3):402–410
7. Hargreaves DJ (1991) Surface waviness effects on the load carrying capacity of rectangular slider bearings. Wear 145:137–151
8. Etsion I (2005) State of the art in laser surface texturing. J Tribol 127:248–253
9. Oliveira JFG, Bottene AC, Franca TV (2011) A novel dressing technique for texturing of ground surfaces. CIRP Ann Manuf Technol 59:361–364. doi:10.1016/j.cirp.2010.03.119
10. Lu X, Khonsari MM (2007) An experimental investigation of dimple effect on the Stribeck curve of journal bearings. Tribol Lett 27:169–176
11. Stepien P (2008) Deterministic and stochastic components of regular surface texture generated by a special grinding process. Wear 271:514–518. doi:10.1016/j.wear.2010.03.027
12. Burton RA (1963) Effects of two dimensional, sinusoidal roughness on the load support characteristics of lubricating film. J Basic Eng 84:258–264
13. Mitsuya Y, Fukui S (1986) Stokes roughness effects on hydrodynamic lubrication. Part I—Comparison between incompressible and compressible lubricating films. J Tribol 108:151–158
14. Tonder K (1995) Dynamics of rough slider bearings: effects of one sided roughness/waviness. Tribol Int 29(2):117–122
15. Letalleur N, Plouraboue F, Prat M (2002) Average flow model of rough surface lubrication: flow factors for sinusoidal surfaces. J Tribol 124:539–546
16. Phuoc Huynh B (2005) Numerical study of slider bearing with limited corrugation. ASME J Tribol 127:582–595
17. Burstein L (2006) Two sided surface roughness and hydrodynamics pressure distribution in lubricating films. Lubr Sci 19(2):101–112
18. Burstein L (2008) Effect of sinusoidal roughened surfaces on pressure in lubricating film. Int J Surf Sci Eng 2(1-2):52–70
19. Kumar R (2008) Studies of the hydrodynamic bearings with surface profiling and entrained solid particulate. Ph.D. Thesis, IIT Delhi
20. Buscaglia GC, Ciuperca I, Jai M (2005) The effect of periodic textures on the static characteristics of thrust bearings. J Tribol 127:899–902

21. Rahmani R, Shirvani A, Shirvani H (2007) Optimization of partially textured parallel thrust bearings with square-shaped micro-dimples. Tribol Trans 50:401–406
22. Murthy AN, Etsion I, Talke FE (2007) Analysis of surface textured air bearing sliders with rarefaction effects. Tribol Lett 28:251–261
23. Tala-ighil N, Maspeyrot P, Fillon M, Bounif A (2007) Effects of surface texture on journal bearing characteristics under steady state operating conditions. Proc Inst Mech Eng, Part J J Eng Tribol 221(6):623–633
24. Sinanoglu C (2009) Investigation of load carriage capacity of journal bearings by surface texturing. Ind Lubr Tribol 61(1):261–270
25. Tonder K (2001) Inlet roughness tribodevices: dynamic coefficient and leakage. Tribol Int 34(12):847–852
26. Cupillard S, Glavatskih S, Cervantes MJ (2008) CFD analysis of journal bearing with surface texturing. Proc Inst Mech Eng, Part J J Eng Tribol 222:97–107
27. De Kraker A, Ostryen RAJ, Van Beek A, Rixen DJ (2007) A multiscale method modelling surface texture effects. J Tribol 129:221–230
28. Brizmer V, Kligerman Y, Etsion I (2003) A laser surface textured parallel thrust bearing. Tribol Trans 46(3):397–403
29. Sahlin F, Glavatskikh S, Almqvist T, Larsson R (2005) Two dimensional CFD analysis of micro patterned surfaces in hydrodynamic lubrication. J Tribol 127(1):96–102
30. Fowel M, Olver AV, Gosman AD, Spikes HA, Pegg I (2007) Entrainment and inlet suction: two mechanisms of hydrodynamic lubrication in textured bearings. J Tribol 129:336–347
31. Arghir M, Roucou N, Helene M, Frene J (2003) Theoretical analysis of the incompressible laminar flow in a macro-roughness cell. J Tribol 125(2):309–318
32. Cupillard S, Glavatskih S, Cervantes MJ (2008) Pressure build up mechanism in a textured inlet of a hydrodynamic contact. J Tribol 130(2):97–107
33. Brajdic-Mitidieri P, Gosman AD, Ioannides E, Spikes HA (2005) CFD analysis of a low friction pocketed pad bearing. J Tribol 127(4):803–812
34. Etsion I (2010) Laser surface texturing and applications. In: Nikas, GK (ed), Recent developments in wear prevention, friction and lubrication, pp 137–157
35. Gupta SL, Kumar V (2003) Handbook of electronics, 31st edn. Pragati Prakashan Publication